UNCLASSIFIED

SECURITY C ...IFICATION OF TH ...AGE (When Data ...ered)

DTIC FILE COPY

(1)

AD-A196 376

REPORT DOCUMENTATION PAGE

READ INSTRUCTIONS BEFORE COMPLETING FORM

REP ... NUMBER: AFIT/CI/NR 88- 81

2. GOVT ACCESSION NO.

3. RECIPIENT'S CATALOG NUMBER

4. TITLE (and Subtitle): A SURVEY OF DIGITAL BEAMFORMING TECHNIQUES AND CURRENT TECHNOLOGY

5. TYPE OF REPORT & PERIOD COVERED: MS THESIS

6. PERFORMING ORG. REPORT NUMBER

7. AUTHOR(s): JOHN EDWARD McCORD

8. CONTRACT OR GRANT NUMBER(s)

9. PERFORMING ORGANIZATION NAME AND ADDRESS: AFIT STUDENT AT: MISSISSIPPI STATE UNIVERSITY

10. PROGRAM ELEMENT, PROJECT, TASK AREA & WORK UNIT NUMBERS

11. CONTROLLING OFFICE NAME AND ADDRESS

12. REPORT DATE: 1988

13. NUMBER OF PAGES: 60

14. MONITORING AGENCY NAME & ADDRESS (if different from Controlling Office): AFIT/NR, Wright-Patterson AFB OH 45433-6583

15. SECURITY CLASS. (of this report): UNCLASSIFIED

15a. DECLASSIFICATION/DOWNGRADING SCHEDULE

16. DISTRIBUTION STATEMENT (of this Report): DISTRIBUTED UNLIMITED: APPROVED FOR PUBLIC RELEASE

DTIC ELECTE AUG 0 3 1988 S D H

17. DISTRIBUTION STATEMENT (of the abstract entered in Block 20, if different from Report): SAME AS REPORT

18. SUPPLEMENTARY NOTES: Approved for Public Release: IAW AFR 190-1
LYNN E. WOLAVER 19 July 88
Dean for Research and Professional Development
Air Force Institute of Technology
Wright-Patterson AFB OH 45433-6583

19. KEY WORDS (Continue on reverse side if necessary and identify by block number)

20. ABSTRACT (Continue on reverse side if necessary and identify by block number): ATTACHED

88 8 ...

DD FORM 1 JAN 73 1473 EDITION OF 1 NOV 65 IS OBSOLETE

UNCLASSIFIED

SECURITY CLASSIFICATION OF THIS PAGE (When Data Entered)

ABSTRACT

Author: John Edward McCord, 2d Lt, USAF

Title of Thesis: Survey of Digital Beamforming Techniques and Current Technology

Degree Awarded: Master of Science, Department of Electrical Engineering, 1987

Institution: Mississippi State University, Mississippi State, Mississippi

Pages in Thesis:

ABSTRACT

Digital beamforming provides key advantages over analog beamforming in radar applications where proper response to multiple jammers in a rapidly changing environment is required. This survey reviews these advantages and various digital methods for attaining them. Disadvantages and limitations are also given. The mathematical basis for beamforming is reviewed. Five experimental digital beamforming systems discussed here reveal the current level of digital implimentation. Also covered are current technologies available and future trends for digital beamforming.

A SURVEY OF DIGITAL BEAMFORMING TECHNIQUES AND CURRENT TECHNOLOGY

by

John Edward McCord

A Thesis
Submitted to the Faculty of
Mississippi State University
in Partial Fulfillment of the Requirements
for the Degree of
Master of Science in the
Department of Electrical Engineering

Mississippi State, Mississippi

December 1987

A SURVEY OF DIGITAL BEAMFORMING TECHNIQUES AND CURRENT TECHNOLOGY

by

John E. McCord

APPROVED:

Frank Ingels
Professor of Electrical Engineering (Chairman of Supervisory Committee and Director of Thesis)

Frank Ingels
Graduate Coordinator
Department of Electrical Engineering

Walter R. Garner
Director of Graduate Instruction
College of Engineering

Willis L. McDaniel
Dean of The College of Engineering

Charles Scott
Acting Associate Vice-President
for Academic Affairs

ACKNOWLEDGEMENTS

I wish to acknowledge with deep appreciation the direction and encouragement I received from Dr. Frank Ingels in this endeavor. Special thanks go to Ann Robertson for her help in typing this thesis. Finally, and most importantly, I wish to thank my family for their continued support, encouragement and prayers during my preparation of this thesis.

John E. McCord

Mississippi State University

1987

ABSTRACT

John E. McCord, Master of Science, December 1987

Major: Electrical Engineering, Department of Electrical Engineering

Title of Thesis: Survey of Digital Beamforming Techniques and Current Technology

Directed by: Franklin M. Ingels

Pages in Thesis: 60 Words in Abstract: 75

ABSTRACT

Digital beamforming provides key advantages over analog beamforming in radar applications where proper response to multiple jammers in a rapidly changing environment is required. This survey reviews these advantages and various digital methods for attaining them. Disadvantages and limitations are also given. The mathematical basis for beamforming is reviewed. Five experimental digital beamforming systems discussed here reveal the current level of digital implementation. Also covered are current technologies available and future trends for digital beamforming.

TABLE OF CONTENTS

TABLE OF CONTENTS (continued)

LIST OF FIGURES

LIST OF TABLES

CHAPTER 1

BASIC PRINCIPLES OF DIGITAL BEAMFORMING

1.0 INTRODUCTION

This paper will concentrate on digital beamforming in the receive mode for uniformly spaced, linear array antennas. While a beampattern for a transmitted signal is described by its power distribution in space, the received beampattern is seen as the antenna response. The two-fold aim of the receiver/beamformer is to optimize the desired signal and minimize undesired interference (i.e., noise, clutter, jamming) [1]. A basic beamformer and control system [2] (Figure 1-1) consists of the antenna elements, the beampattern controller, and the beamformer. An incident signal wavefront induces linear phase errors (delays) across the array of antenna elements (i.e., the aperture). The system removes these phase shifts from the desired direction and accumulates the desired signals. The beampattern controller determines weighting coefficients to be applied to the input signals of each element to minimize phase and amplitude errors between elements, to steer the beam in the direction of a desired signal, to control sidelobe levels and null placements, and/or to produce multiple beams for simultaneous tracking of several targets. The beamformer combines the input signals and the weighting coefficients to produce the input beam for radar processing.

The main advantages of digital beamforming are

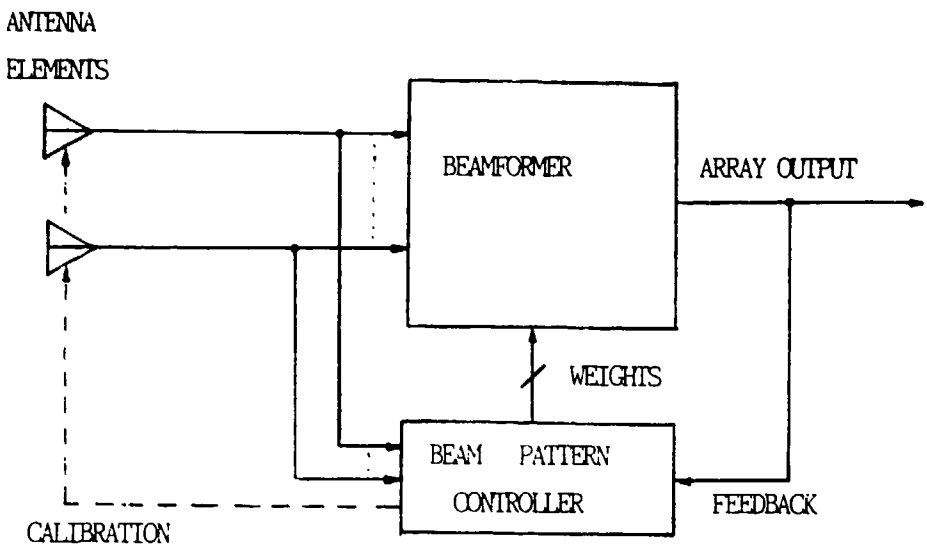

Figure 1-1. Basic beamformer and control system.

. Antenna self-calibration for ultra-low sidelobes,

. Improved adaptive beamforming,

. More closely spaced, multiple beams,

. Array element pattern correction, and

. Superresolution.

The major disadvantages are circuit complexity, cost and processing time.

1.1 ANTENNA SELF-CALIBRATION FOR ULTRA-LOW SIDELOBES

To apply calibration techniques, a test signal is applied to the input receivers, on an occasional basis, and then measured internally to offset channel matching errors. This insures that the required beam shape and pointing angle (as measured from the perpendicular axis of the array face) is maintained. If the test signal is applied to the antenna elements (by either a near or far-field auxiliary antenna or precise coupling lines across the antenna face), then additionally, the antenna and feed path errors are also offset. For a test signal applied to each element, $[x'_1, x'_2, \ldots, x'_n] = X'$, the response is $[x''_1, x''_2, \ldots, x''_n] = X''$. A diagonal matrix operator C is formed such that

$$c_{rr} = \frac{x'_r}{x''_r} \quad , \qquad r = 1,2,\ldots,n \quad . \qquad 1\text{-}1$$

This matrix is applied to the normal weight vector W which modifies the input signals, so that the input beam shape and pointing angle are now modified by the weight vector CW. Problems can arise from improper placement of the auxiliary antenna. Correct directivity must be insured so that the array is illuminated without illuminating nearby structures, which can return undesired echoes. Also, the auxiliary antenna must be physically placed to prevent it from being a source of unwanted echo, thus disturbing the field distribution. With calibration, a clearer beam is formed with sharper nulls and there is better sidelobe control. The system is not misled by distortion, and therefore, responds more rapidly and smoothly as it steers the beam. Also, if individual elements fail, the self-calibration will minimize the effect on the whole system. Finally, self-calibration can provide an on-line maintenance check of individual elements. If an element's performance drops below a predetermined level, the operator can be notified.

1.2 ADAPTIVE BEAMFORMING

The second advantage, adaptive beamforming, may well be the best exploitation of digital implementation. This technique of effective sidelobe control and null steering utilizes adaptive weight formation. Properly determined weights applied to the input element signals form null patterns with very low sidelobes in the direction of unwanted noise sources. The null depths are not affected by the amplitude and phase errors in the element and channel paths. Barton [2] points out

that because of this, adaptive weight control competes with calibration techniques in the job of null steering. This is apparent since reducing amplitude and phase errors by calibration will not appreciably enhance adaptive weight control. Therefore, it is not cost effective (at least at present) to employ both techniques in one system.

The general idea of adaptive weight control is to determine the weights necessary for each element such that the beampattern formed has nulls in the direction of interference (i.e., clutter, jammers, etc.). Thus, with updated returns the beam controller discerns between interference and the desired signal, so as to degrade (or pre-whiten) the unwanted signals and enhance the beam response to the desired signals.

There are several general approaches (or methods) to adaptive beampattern control. One of the earliest is the Applebaum-Howells [3,4] (Figure 1-2) method which uses a closed-loop control system incorporating an externally provided steering vector through auxiliary receiving antenna elements. Sidelobe cancellation circuits drive the weighting networks toward weight values that minimize interference levels at the output. This iterative method was initially intended for an analog system. Closely related is the Widrow LMS adaptive array shown in Figure 1-3 [5]. This time-sampled digital method uses a steepest descent method of solving a least mean squares (LMS) error problem, sometimes called a conjugate-gradient method. It minimizes the effect of the interference at the beamformer output through an iterative scheme. The path of steepest descent is based on some measurement of the rate of change of output interference as a function of the in-phase and quadrature components of the weighting

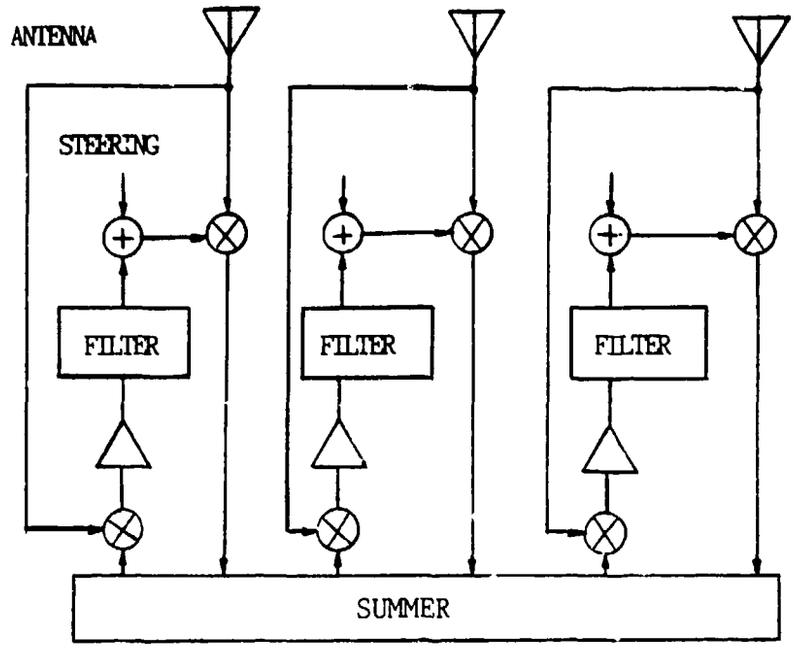

Figure 1-2. Applebaum-Howells adaptive array.
(Taken from reference 4, page 32-43)

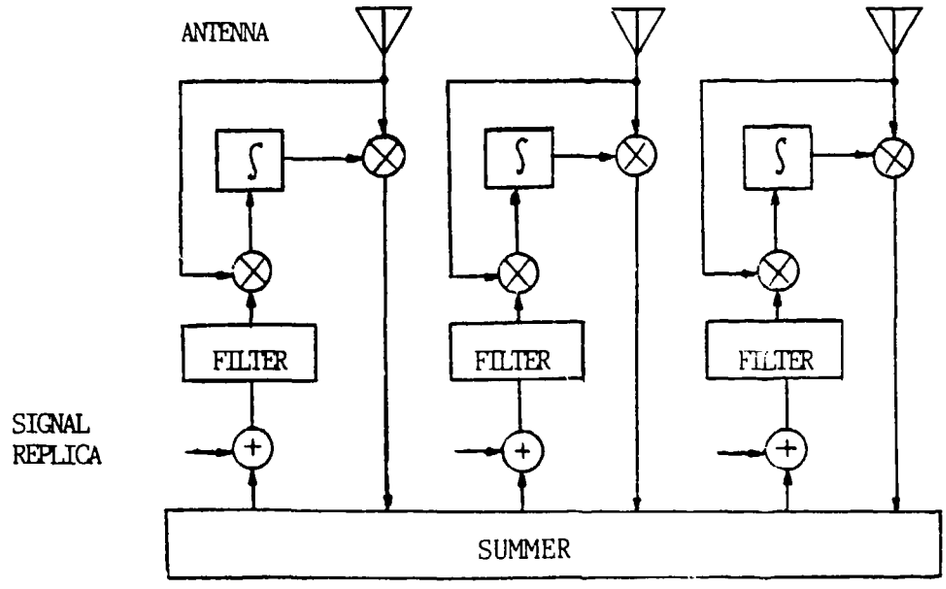

Figure 1-3. Widrow LMS adaptive array.
(Taken from reference 4, page 32-44)

coefficients. A variation of Widrow's LMS array is the weight perturbation method proposed by Hudson and Cantoni, which also obtains adapted weights using the steepest descent method. Here a specially selected perturbation or change of the beamformer's output weights is applied, and the resulting change in output noise is measured. This procedure is repeated until it converges to the weights which will minimize the effect of interference. Unlike in the Widrow and Applebaum-Howells methods, time samples of the input element signals are not used. The biggest problem with these three iterative methods is the slow rate of convergence in cases of unfavorable distributions in jammer powers and directions.

The next method involves the direct evaluation of the optimum weights from a measurement of the covariance matrix of the interference signals from the individual array elements. Compton refers to this as a power inversion array, while Brennan and Reed call it a sampled matrix inversion (SMI) [6] array. This method requires digital control using complex matrix arithmetic. The input noise field is sampled N times with the desired signal absent such that $x^{(j)}$ for $j = 1,2,\ldots,n$ denotes the jth sample of vector x. The estimated covariance matrix is defined as

$$M = \langle (X^{(j)})^{*} (X^{(j)})^{T} \rangle \quad , \qquad 1\text{-}2$$

which contains the values of interference correlation between all the receive elements. This covariance matrix is then inverted and post-multiplied by a vector representing the desired look direction. The resulting vector has the required weights to minimize interference or

jammers and optimize reception of the desired signals. Problems with the SMI method involve complexity of the processor and the high data rate required to operate in real-time. The number of floating point operations (i.e., computer multiplication and division) is approximately $(7/6)N^3$, where N is the number of channels. Therefore, if the jamming environment changes rapidly with time, the number of elements, N, will be restricted by the available speed of the processor. Nonetheless, the SMI method is orders of magnitude faster than the iterative schemes discussed earlier. For large arrays, sub-arraying techniques can be applied to reduce the dimensionality of an NxN array into N linear arrays, making a digital solution feasible.

Another approach to adaptive beamforming is put forth by Hung and Turner [7]. Here it is assumed that the array has a large number of elements, N, compared to the number of jammers, L, that the radar is designed to suppress. To suppress L jammers, M noise samples denoted by $\{U_1, U_2, \ldots, U_m\}$ are required, where L and M are approximately equal. If $M < L$, the first M strongest jammers are suppressed. The jammer power is usually reduced to a few dBs above the white noise level. This algorithm requires $(4M^2 + 6M + 2)N$ real adds and $(4M^2 + 8M + 4)N$ real multiply operations. The algorithm proceeds as follows:

Step 1 Calculate the power of the first noise vector

$$|U_1|^2 \quad .$$

(Steps 2 to 9 use Gram-Schmidt decomposition to construct an orthogonal basis set,

$\{V_1, V_2, \ldots, V_M\}$, M = number of noise samples. For the jammer vectors, the threshold Δ is the noise level below which the vector is considered jammer-absent.)

Step 2 Form the normalized basis vector as

$$V_1 = \begin{cases} U_1/|U_1| & , \quad |U_1|^2 > \Delta \\ 0 & , \quad |U_1|^2 \leq \Delta \end{cases} .$$

Step 3 Set m = 2.

Step 4 Calculate U_m as

$$U_m = U_m - \sum_{m=1}^{m-1} (V_m^T . U_m) V_m .$$

Step 5 Calculate $|U_m|^2$.

Step 6 Calculate V_m as

$$V_m = \begin{cases} U_m/|U_m| & , \quad |U|^2 > \Delta \\ 0 & , \quad |U|^2 \leq \Delta \end{cases} .$$

Step 7 If m = M, go to Step 10.

Step 8 Replace m by m + 1.

Step 9 Return to Step 4.

Step 10 The quiescent weight vector W_q is represented by its two orthogonal components W^{11}_Q and W^0_λ, such that W^{11}_Q is in the subspace spanned by the basis vector V

(where $W^{11}{}_Q{}^T V = W_2{}^T V$), and $W^0{}_Q$ is in the subspace orthogonal to V (where $W^0{}_Q V = 0$). Calculate $W^0{}_Q$ as

$$W^0{}_Q = W_Q - \sum_{m=1}^{M} (V_m{}^T W_Q) V_m \quad .$$

Step 11 Calculate the adjusted weight vector W_a as

$$W_a = W^0{}_Q / |W^0{}_Q| \quad .$$

The Hung and Turner algorithm is much faster than previous methods discussed. For the example of a 1000-element array with the ability to suppress 10 jammers, this method requires less than 5×10^5 multiplications compared to the SMI's requirement of 10^9 multiplications. Hung's method is limited by how rapidly the jammer environment is changing and, therefore, how often updated weights are needed, but appears to offer the best approach for adaptive nulling.

The final adaptive digital beamforming scheme to be reviewed, based on the work of Ward, Hargrave and McWhirter, implements a systolic array of parallel processing nodes to perform their data domain algorithm [8,9]. This algorithm produces the desired beampattern without explicitly forming the adaptive weight vector. If the desired signal is called vector y and the weighted array input is called $\bar{\bar{X}}\bar{\bar{W}}$, then the problem becomes the error minimization $\bar{e} = \bar{\bar{x}}\bar{w} - \bar{y}$. The vector $\bar{w}$ which gives the smallest vector $\bar{e}$ has the desired weights (Figure 1-4). In the SMI (sampled matrix inversion) method, this weight vector is found by

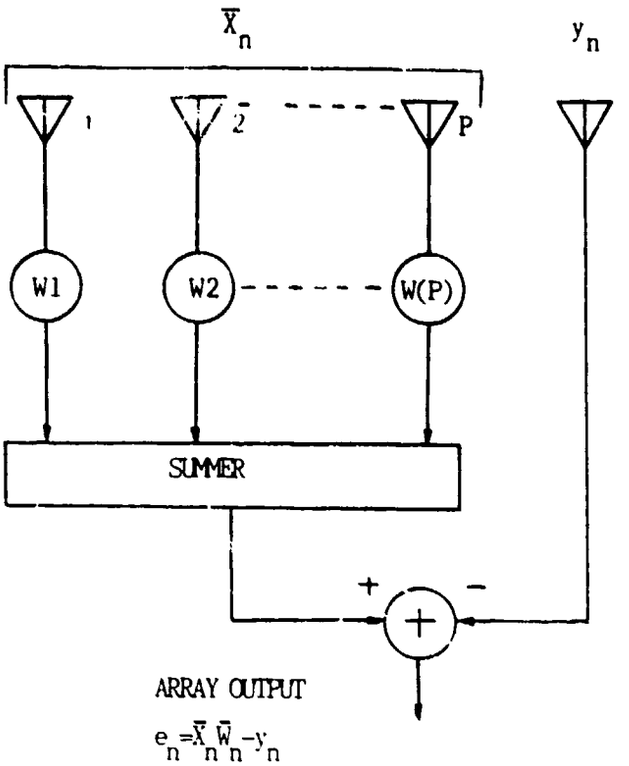

$$\bar{X}_n = \begin{bmatrix} \bar{X}^T(t_1) \\ \bar{X}^T(t_2) \\ \\ \\ \bar{X}^T(t_n) \end{bmatrix}, \qquad y_n = \begin{bmatrix} y(t_1) \\ y(t_2) \\ \\ \\ y(t_n) \end{bmatrix}$$

Figure 1-4. Adaptive array notation.
(Taken from reference 8, page 302)

forming the covariance matrix, inverting it, and multiplying it by the desired look direction vector. This procedure is not only mathematically intensive, but requires very precise arithmetic to prevent numerical instability when the input set of linear equations are poorly conditioned. This instability can result because the covariance matrix involves squaring data (actually multiplying data with its conjugate). To avoid this, the data domain algorithm of Hargrave and Ward applies a series of Givens rotations to time sampled data (producing a Q-R decomposition). The Givens rotation behaves as follows:

$$\begin{bmatrix} C & -S \\ S & C \end{bmatrix} \cdot \begin{bmatrix} X_{11} & X_{12} & \cdots & X_{1n} \\ X_{21} & X_{22} & \cdots & X_{2n} \end{bmatrix} = \begin{bmatrix} X'_{11} & X'_{12} & \cdots & X'_{1n} \\ 0 & X'_{22} & \cdots & X'_{2n} \end{bmatrix}$$

As illustrated in Figure 1-5, a new row of data is applied to the triangular array. The Givens rotation drives the component on the left of the previous data row to zero. This modified vector, reduced in length, is passed to the next row of processors, where the Givens rotation is applied again. This is repeated until all but one component has been driven to zero and the array has been effectively updated. At each step, new data is entered at the top. The final component at the array output is a scaled version of the desired beamformed output that would have been obtained by applying the weight vector to the signal vector. Therefore, the weight vector is not derived explicitly.

Each node of the systolic array needs to be an advanced programmable digital signal processor chip with direct float-point

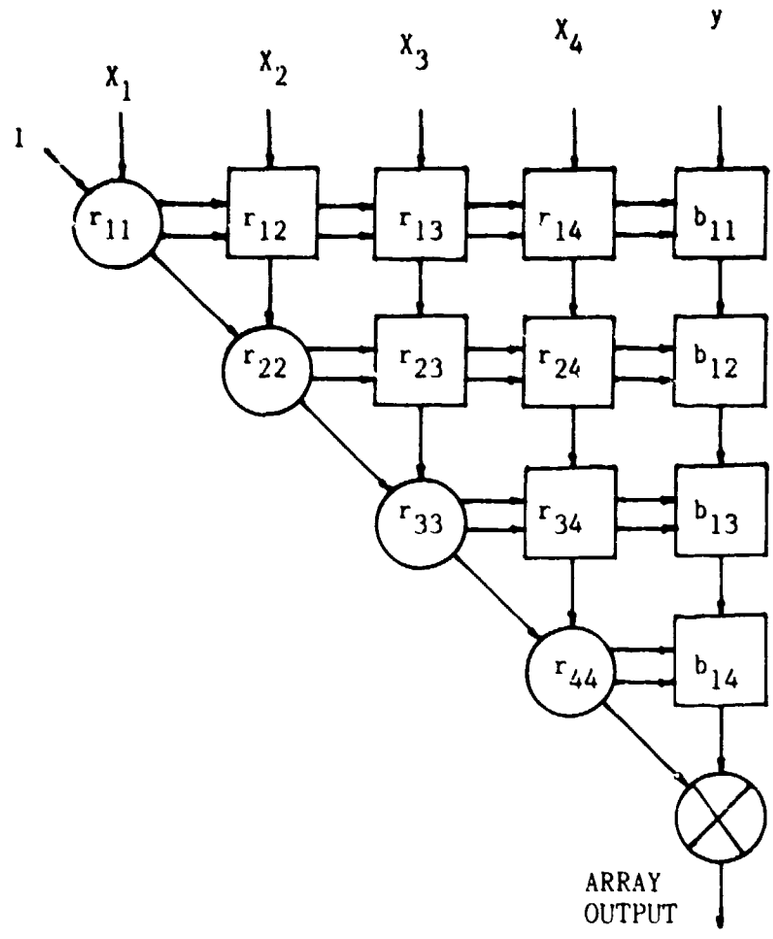

Figure 1-5. Systolic array for adaptive beamforming.
(Taken from reference 8, page 304)

capability. Even so, the operational bandwidth is limited (at the present) to 10 MHz, at which frequency each node processor must perform its function within a single Nyquist sampling period of about 50 to 150 ns for real-time operation. Cost and physical space restrictions will limit the antenna array size. Advances in VLSI (very large scale integration) will be needed for practical implementation of a systolic array.

1.3 CLOSELY SPACED MULTIPLE BEAMS

Multiple beams allow parallel operation and higher data rates than possible with a single beam, giving faster assessment of the desired region. A phase array antenna with N elements is theoretically able to form N independent beams simultaneously from a single aperture . Figure 1-6 shows simultaneous three-beam formation using three phase shifters per element [10]. To form k beams in an n element array ($k \leq n$) would require nk phase shifters. This obviously would be a costly and complex system for other than just a few beams. This antenna is referred to as a post-amplification beamforming array. Another analog multiple beam antenna is the Blass beamforming array. Here delay lines are tapped at appropriate points to form beams at the desired angles. One Blass application used 30 miles of s-band waveguide as delay lines to form 333 independent beams at various elevation angles. The Butler beamforming array can form n beams from n elements when n can be expressed as some power of two ($n = 2^p$). Figure 1-7 shows an 8-element, 8-beam Butler matrix.

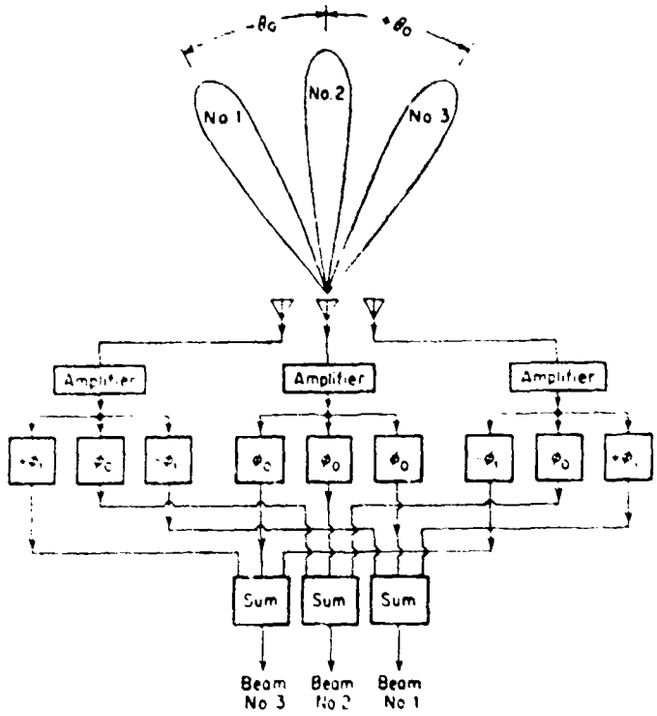

Figure 1-6. Simultaneous postamplification beam formation. (Taken from reference 10, page 311)

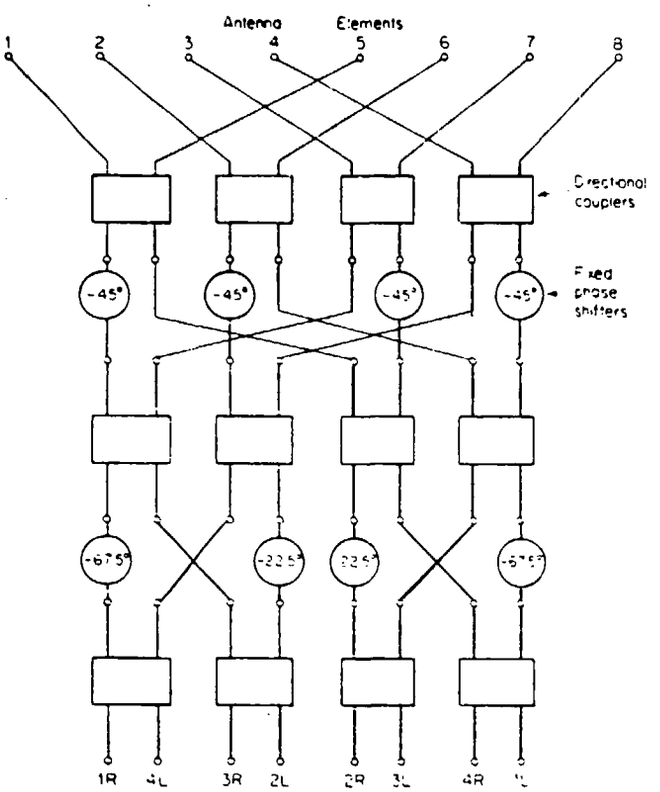

Figure 1-7. Eight-element Butler beamforming matrix. (Taken from reference 10, page 313)

These three analog multiple-beam formers can also be implemented digitally. Once the input signals at each element have been digitized, the signal-to-noise ratio (SNR) is set, and weights can be applied to form as many beams as desired with no restriction on their mutual characteristics. In contrast, RF beamformers must satisfy a minimum spacing criterion due to the requirement that all beams be mutually orthogonal (i.e., ''The average value over all angles of the product of one beam response with the conjugate of the other must be zero'') [2]. This arbitrary weighting to form k simultaneous beams requires $4nkf_r$ real multiplications per second when sampling is performed at f_r Hz (n equals the number of elements and 4 real multiplications are needed for each complex multiplication). As the number of beams desired, k, approaches n, the number of complex multiplications per sample approaches n^2. Thus for a large array the circuit complexity and processing time may be unmanageable. In these cases, a Fourier Transformation Process can be used to form an entire set of n beams [11,12,13,14]. If the discrete Fourier Transform (DFT) is used, which is analogous to the Blass beamformer, then $4n^2$ real multiplications are required. A faster, more economical algorithm called the Fast Fourier Transform (FFT) reduces the number of real, non-trivial multiplications to $[2n(\log_2 n-3) + 8]$ (for the Radix-2 Cooley-Tukey FFT). The FFT is analogous to the Butler beamformer. There are other FFT techniques, such as the Winograd FFT, which offer even greater efficiency under certain circumstances. The Winograd FFT can perform the same transform using one-fifth the multiplications of the Radix-2 FFT. The Fourier Transform method of multiple beamforming

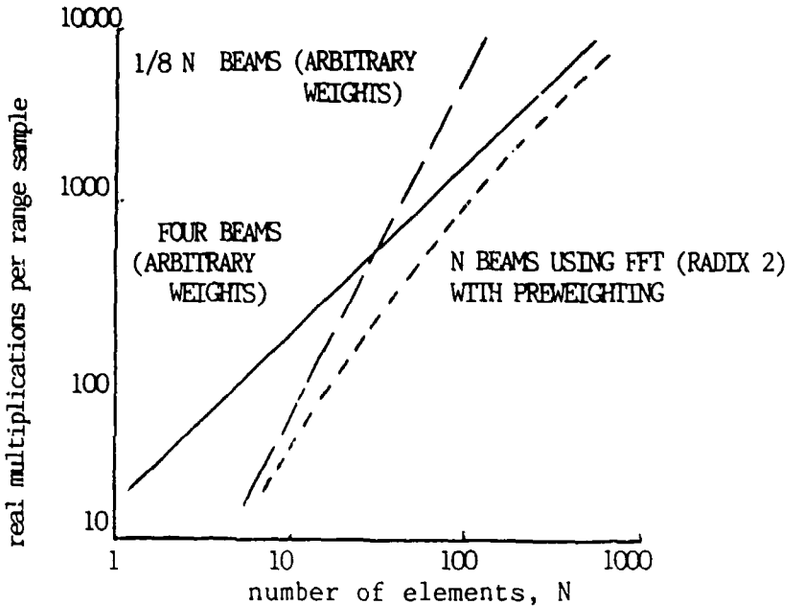

Figure 1-8. Number of multiplications per range sample for different beamforming configurations. (Taken from reference 2, page 272)

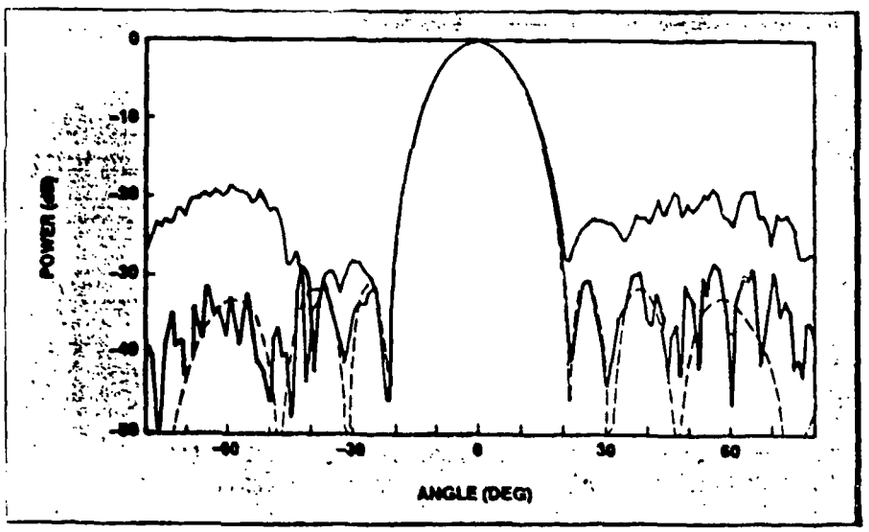

Figure 1-9. Coupling effects in eight-element array. Upper and lower solid curves show measured 30 dB Chebyshev patterns below and after mutual coupling correction. Dashed line shows ideal pattern.
(Taken from reference 1, page 112)

differs in performance from the custom beams formed by arbitrary weights. Arbitrary weights allow arbitrary beam patterns and directions, whereas the DFT/FFT produce identical beams spaced according to the orthogonality constraint. Figure 1-8 compares the number of real multiplications per range sample to the number of elements for a four-beam arbitrarily weighted pattern, to (1/8) n beams using arbitrary weights, and to the Radix-2 FFT with pre-weighting.

1.4 ARRAY ELEMENT PATTERN CORRECTION

Digital beamforming also allows the correction of undesired coupling effects of neighboring elements on an individual element. The received signal at an element is comprised of the direct principal plane wave and small signals due to scattering of the principal plane wave on neighboring elements. For a linear array, if the received signal vector is $\bar{X}$, and the desired signal vector is $\bar{X}_D$, then these can be related by a multiplying matrix C, such that $\bar{X} = C\bar{X}_D$, and consequently, $\bar{X}_D = C^{-1}\bar{X}$. Therefore, the coupling correction can be achieved by multiplying the input signal vector by the inverse coupling matrix C^{-1}. This results in improved pattern control and lower sidelobe levels. Figure 1-9 shows the effects of the coupling corrector on an eight-element array, reducing the sidelobe level from -20 to -30 dB.

1.5 SUPERRESOLUTION

Resolution is the ability of a radar to distinguish between two or more targets whose parameters (range, doppler, etc.) are nearly equal in value. Conventional resolution is the beamwidth of the summed beam, which is limited by the array aperture . Superresolution is based on the idea that multiple spatial samples of the incoming wavefront provide additional information, and that some assumptions about the signal can be made. Nickel (et.al) indicates that the lower limit on superresolution seems to be two targets separated by a quarter-beamwidth [15]. He has data to indicate that the limit is more determined by channel mismatch errors than by pure signal-to-noise ratio, as reported by Steyskal. Superresolution methods involve highly complex non-linear signal processing algorithms which will require a parallel beamformer, a systolic array processor for Q-R decomposition, or a systolic array processor for singular value decomposition (depending on the actual algorithm selected). Superresolution techniques would not replace conventional resolution techniques, but provide an additional refinement when needed.

In concluding this section on the benefits of digital beamforming, it should be stated that the major area of application at the present involves beam control and sidelobe control. As alluded to earlier, one system would not incorporate all functions discussed.

1.6 CHARACTERISTICS OF THE INPUT CHANNEL

In an analog system, the signals from each element pass through a phase shifter to remove the phase delay accumulated across the array face, and to steer the beam in the desired look direction. These signals are then summed to produce one input beam which is routed to the radar processor.

In a digital receiver, the input element signal is either down-converted to some non-zero intermediate frequency (i.f.), sampled, and digitized by a single analog-to-digital converter (ADC), or down-converted to zero i.f. (baseband) in-phase and quadrature channels, sampled and digitized by two ADC's. Barton points out that the extra hardware in the second case is more than compensated for by the improvement in the net sampling rate [2]. For a typical radar pulse spectrum with a 3 dB spectrum width B, the sampling rate for the single ADC is 5.4B, while for the pair of ADC's at baseband, the sampling rate is 1.4 B (see Figure 1-10). A diagram of this input circuit is shown in Figure 1-11.

1.7 CHARACTERISTICS OF THE DIGITAL BEAM PATTERN CONTROLLER

Where phase shifters are used in an analog system to remove phase errors and provide beam steering, the digital system uses a waveform digital matched filter processor to perform phase rotation arithmetic at each element. The digital representation provides much greater

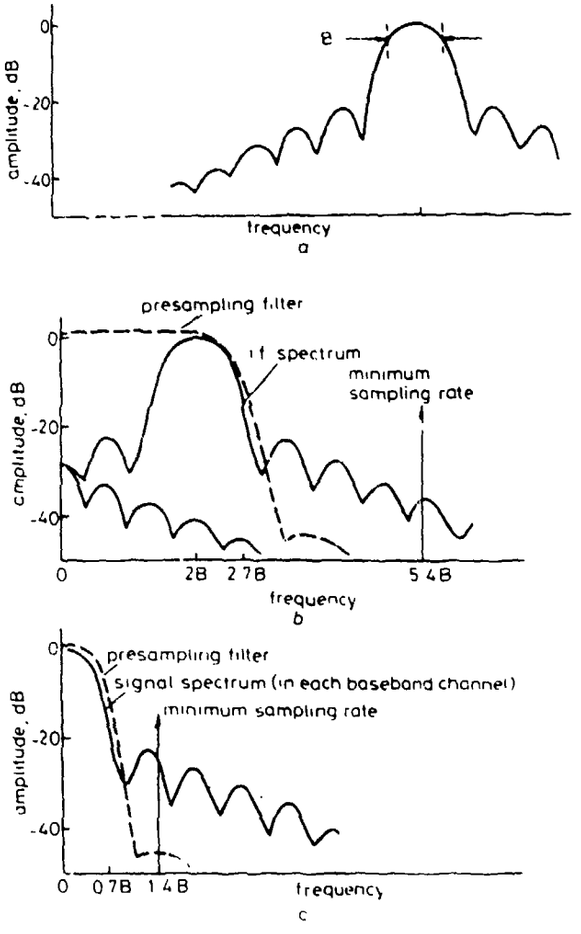

Figure 1-10. Sampling a typical radar pulse spectrum. The pulse in (a) is shown downconverted to a non-zero i.f. (b), and baseband frequency (c). (Taken from reference 2, page 268)

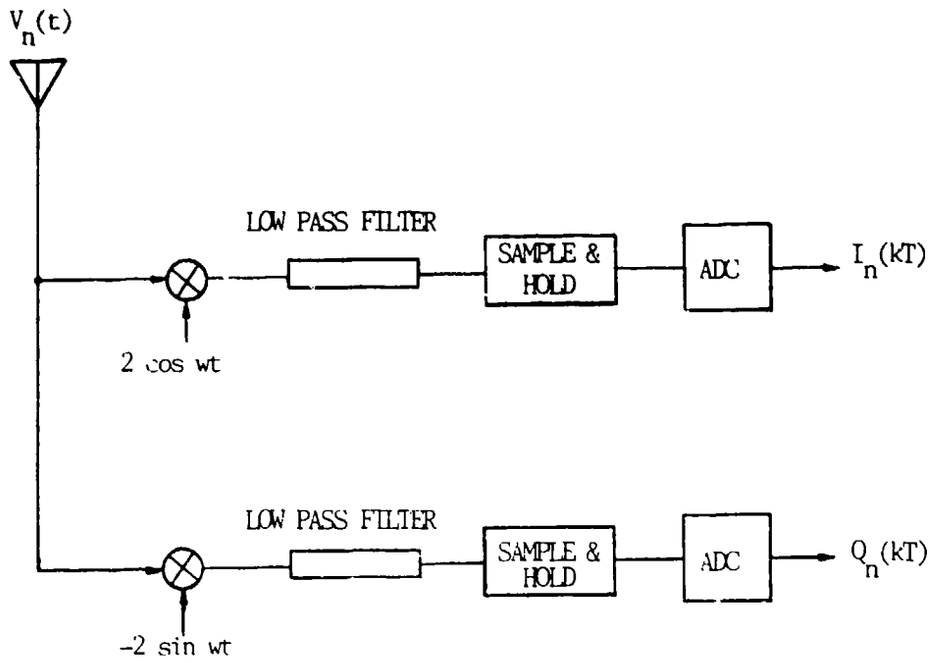

Figure 1-11. Basic input circuit with dual ADCs.

flexibility in signal manipulation and control due to algorithms which can be applied.

Two characteristics that are important in antenna systems are dynamic range and signal bandwidth. The dynamic range of a digital beamformer and controller is determined by the number of bits B in the ADC, and the number of parallel channels N. Let A be the maximum amplitude of the ADC of each channel. Then the total amplitude is NA, and the maximum power is

$$P_{max} = \frac{(NA)^2}{2} \quad . \qquad 1\text{-}3$$

Each channel has a minimum power,

$$P_{n,min} = \frac{A^2}{2^{B-1}} \quad , \qquad 1\text{-}4$$

and, therefore, the summed P_{min}, assuming the threshold is set to where the average of half the channels are triggered by thermal noise, is

$$P_{min} = \frac{N}{2} \cdot \frac{A^2}{2^{(B-1)2}} \quad . \qquad 1\text{-}5$$

The dynamic range, then, is

$$\frac{P_{max}}{P_{min}} = 2^{2(B-1)} N \quad ,$$

$$= [6(B-1) + 10\log_{10}N] \text{ dB} \quad . \qquad 1\text{-}6$$

So it may be seen that the dynamic range increases 6 dB per bit. N expresses the gain due to ''coherent integration'' of the N elements. Limitations to dynamic range are: thermal noise, in-phase and quadrature orthogonality errors, quantization errors, sampling time jitters, and linearity errors.

Signal bandwidth is constrained by the ADC sampling rate and the processing speed of the beamformer. More will be said when hardware requirements are exrmined.

CHAPTER 2

MATHEMATICAL BASIS OF BEAMFORMING

2.0 INTRODUCTION

This chapter will develop the mathematical basis of forming a single beam, steering the beam, making beam corrections, and forming multiple beams [16]. Signal representation in the digital domain will also be examined.

2.1 FORMING A SINGLE BEAM

Consider beamforming with the 2-element array shown in Figure 2-1. A far field wavefront (i.e., planar) arrives at each sensor with a time delay at sensor 0, relative to sensor 1, of: $\tau = d\sin\theta/c = d\sin\theta/\lambda f$ (sec), where c = speed of light. The phase shift of the voltage at sensor 0, relative to sensor 1, is

$$\phi = \frac{2\pi d\sin\theta}{\lambda} \quad \text{(radians)} \quad . \qquad 2\text{-}1$$

Let the received voltage at sensor 1 be $e^{j\omega t}$. Then the normalized voltage at the summer output is

$$v = e^{j\omega t} + e^{j(\omega t-\phi)} = e^{j\omega t}(1+e^{-j\phi}) \quad . \qquad 2\text{-}2$$

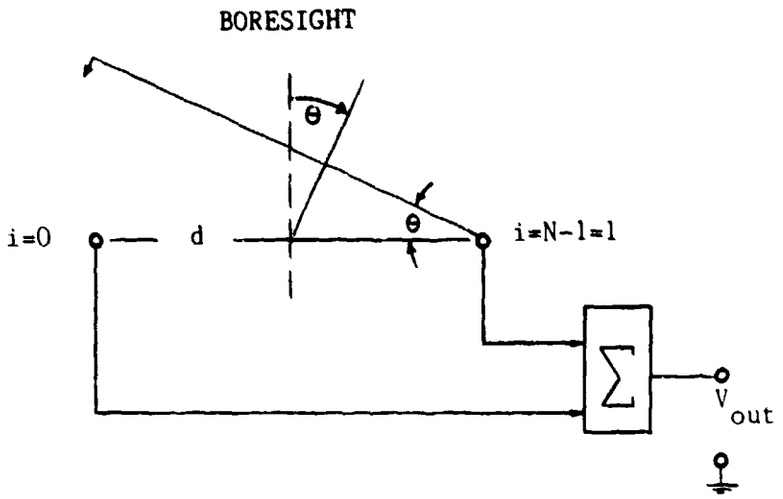

Figure 2-1. Two-element array.
(Taken from reference 16, page 1)

To find |v|, this equation may be manipulated as follows:

$$ve^{-j\phi} = e^{j\omega t}\,(e^{-j\phi} + e^{-j2\phi}) \quad . \qquad 2\text{-}3$$

Subtracting the first equation from the second provides

$$v(e^{-j\phi} - 1) = e^{j\omega t}(e^{-j\phi} + e^{-j2\phi} - 1 - e^{-j\phi}) . \qquad 2\text{-}4$$

$e^{-j\phi}$ cancels, leaving

$$v = e^{j\omega t}\ \frac{e^{-j2\phi} - 1}{e^{-j\phi} - 1} \quad ,$$

$$v = e^{j\omega t}\ \frac{e^{-j\phi}\,(e^{-j\phi} - e^{j\phi})}{e^{-j\phi/2}\,(e^{-j\phi/2} - e^{j\phi/2})} \quad ,$$

$$v = e^{j\omega t}\ \left(\frac{\sin\phi}{\sin\phi/2}\right) \quad , \text{ with phase angle } (-\phi/2),$$

and, finally,

$$|v| = \frac{\sin\phi}{\sin\phi/2} \quad . \qquad 2\text{-}5$$

This can be expanded to N elements as follows:

$$v = e^{j\omega t} + e^{j(\omega t-\phi)} + e^{j(\omega t-2\phi)} + \ldots + e^{j(\omega t-(N-1)\phi)} \quad ,$$

$$v = e^{j\omega t}(1 + e^{-j\phi} + e^{-j2\phi} + \ldots + e^{-j(N-1)\phi}) \quad ,$$

$$ve^{-j\phi} = e^{j\omega t}(e^{-j\phi} + e^{-j2\phi} + \ldots + e^{-jN\phi}) \quad ,$$

$$v(e^{-j\phi}-1) = e^{j\omega t}(e^{-jN\phi}-1) \quad ,$$

$$v = e^{j\omega t}(e^{-jN\phi}-1)/(e^{-j\phi}-1) \quad ,$$

$$v = e^{j\omega t} \frac{e^{-j\frac{N\phi}{2}}(e^{-j\frac{N\phi}{2}} - e^{j\frac{N\phi}{2}})}{e^{-j\phi/2}(e^{-j\phi/2} - e^{j\phi/2})} \quad ,$$

$v = e^{j\omega t} \left(\frac{\sin N\phi/2}{\sin \phi/2}\right)$ with phase angle $(N-1)\phi/2$, and

$$|v| = \frac{\sin N\phi/2}{\sin \phi/2} \quad . \qquad 2\text{-}6$$

The maximum $|v|$ occurs at $\phi = 0$. Applying L'Hopital's rule, $|v|_{max} = N$. Therefore, the normalized voltage is

$$|v| = 1/N \frac{\sin N\phi/2}{\sin \phi/2} \quad . \qquad 2\text{-}7$$

The beampattern is defined as the square of the normalized voltage response $b(\theta)$ versus θ, so that

$$b(\theta) = \frac{|v|^2}{N^2} = \frac{\sin^2(N\phi/2)}{N^2\sin^2(\phi/2)}, \text{ where } \phi = \frac{2\pi d}{\lambda} \sin\theta \quad . \qquad 2\text{-}8$$

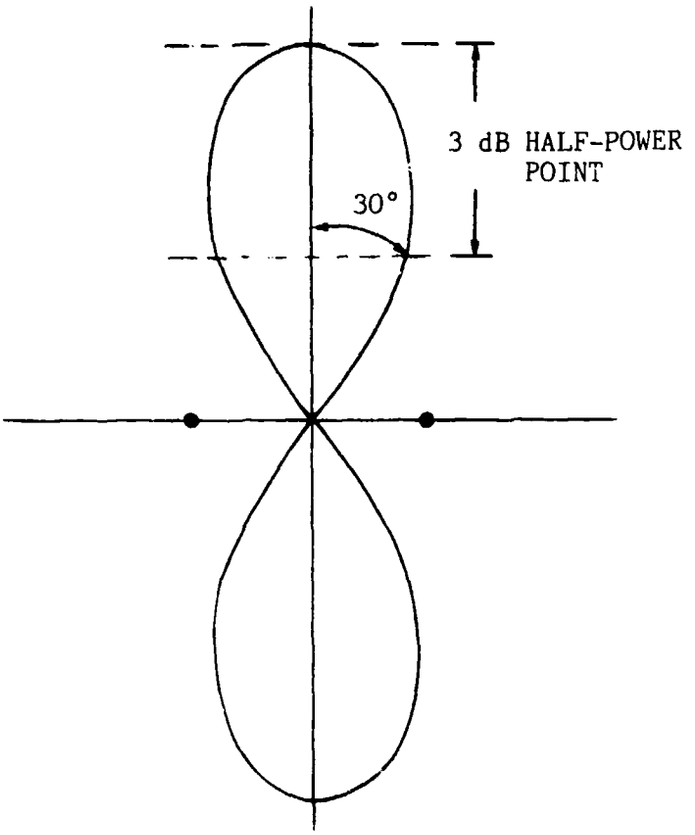

Figure 2-2. Beam pattern for two-element array with $d=\lambda/2$.

For a two element array and $d = \lambda/2$, the beampattern formed is shown in Figure 2-2.

Since $|v|max = N$, then $b(\theta)max = 1$ at $\theta = 0°$. To find $b(\theta)min$, set $b(\theta) = 0$; then it follows that

$$\sin(\frac{N\phi}{2}) = 0, \text{ which is true when}$$

$$\frac{N\phi}{2} = k\pi, \ (k = 0,1,2,\ldots).$$

Letting $k = 1$ and replacing ϕ with $\frac{2\pi d}{\lambda}\sin\theta$ gives

$\frac{2\pi Nd}{2\lambda}\sin\theta = \pi$. It follows that for $b(\theta) = 0$,

$$\theta = \sin^{-1}(\frac{\lambda}{Nd}) \quad . \qquad 2\text{-}9$$

This angle represents the direction of the first null. A third value of interest is the half power beamwidth (HPBW) $b(\theta)_{3dB} = .5$, which occurs when

$$\theta = \frac{1}{2}\sin^{-1}\,[2(.886)/N] \sim 50.9°/N \quad .$$

As the number of equally spaced elements increases, the beam gets narrower. Therefore, the beamwidth, and hence the target resolution, can be controlled by the number of elements used in the array. This is

clearly shown in Table 2-1.

TABLE 2-1. BEAMPATTERN DATA FOR $d = \lambda/2$

N	θ for $b(\theta)_{minimum}$	θ for $b(\theta)_{maximum}$	θ for $b(\theta)_{3dB}$	or $\pm 50.9^{\circ}/N$
2	90°	0°	±30°	±25.45°
3	42°	0°	±18.15°	±16.95°
5	23.5°	0°	±10.4°	±10.18°
7	16.6°	0°	± 7.35°	± 7.27°
12	9.6°	0°	± 4.25°	± 4.24°
50	2.3°	0°	± 1.02°	± 1.02°

2.2 BEAM STEERING

If the signal wavefront arrives at the array with an angle θ greater than $b(\theta)_{3dB}$, much of the signal is lost. Therefore, it becomes necessary to steer the beam to receive maximum signal voltage. This is accomplished by adding phase shifts (or weights) to each element so that all signals reach the summer in phase, producing the maximum input voltage (see Figure 2-3).

The summed voltage is

$$v = \sum_{i=0}^{n-1} S_i C_i = \sum_{i=0}^{n-1} S_i e^{-j(i-n+1)\phi} \quad \text{for } \phi = \frac{2\pi d}{\lambda} \sin\theta \quad . \qquad 2\text{-}11$$

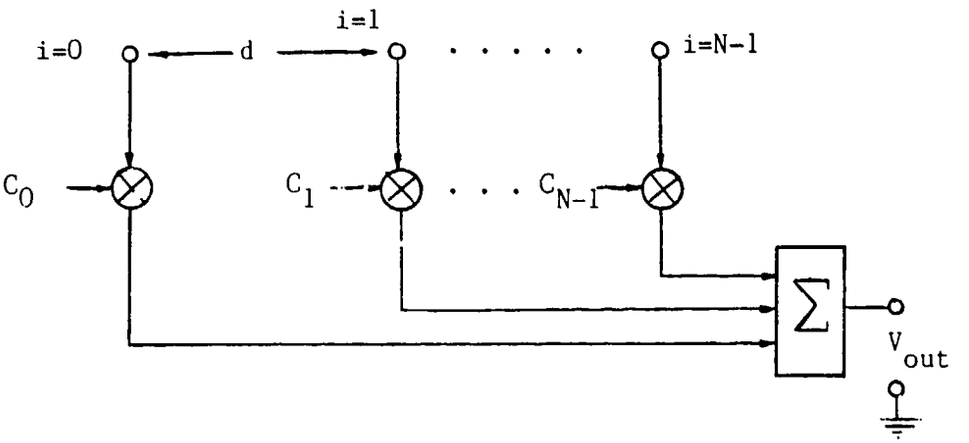

Figure 2-3. Array phase shift weighting.

Now, $S_i = e^{j[\omega t-[(n-1)-i]\phi)}$, and $C_i = e^{j((n-1)-i)\phi}$.

Therefore, the summed voltage of their products is

$$v = e^{j(\omega t-(n-1)\phi)}e^{j(n-1)\phi} + e^{j(\omega t-(n-2)\phi)}e^{j(n-2)\phi}+\ldots+ e^{j\omega t}e^{j0} ,$$

$$v = Ne^{j\omega t} , \qquad 2\text{-}12$$

and the beampattern response is

$$b(\theta) = \frac{|v|^2}{N^2} = \frac{N^2}{N^2} = 1 . \qquad 2\text{-}13$$

Hence, the beam is steered to compensate for the angle ϕ, and is now ''looking'' in the desired direction.

2.3 BEAM CORRECTION

Just as the beam was steered by applying phase shifting (or beamsteering) coefficients to the signals at each element, corrective coefficients may be applied to improve other aspects of the received signal as well.

A target in the near field results in a return wavefront which is not planar, but curved. The center of the curved wavefront arrives earlier than the rest, causing distortion. The closer the target, the more pronounced is the error. A phase lag correction coefficient based on target range can be applied to minimize this error. Let

$$\phi_i(t) = -k[(R^2(t)+x_i^2)^{1/2} - R(t)] \simeq \frac{-kx_i^2}{2R(t)} \text{ if } x_i \ll R(t), \qquad 2\text{-}14$$

where

$k = 2\pi/\lambda$,

$x_i = id$ (i = ith element from center) ,

$R(t)$ = Range of Target .

This correction is referred to as range focusing.

Weighting coefficients W_i are also used to control the sidelobes of the voltage response of each steered beam. These weights adjust the gains of the receiving elements to produce low sidelobes.

The received signal altered by range focusing, beamsteering, and sidelobe shading is

$$B = \sum_{i=0}^{n-1} W_i S_i e^{\frac{kx_i^2}{j2R(t)}} e^{-j(i-n+1)\phi} \quad . \qquad 2\text{-}15$$

This is shown in Figure 2-4.

2.4 MULTIPLE BEAM FORMING

For arbitrary weighting, multiple beams are formed by applying the

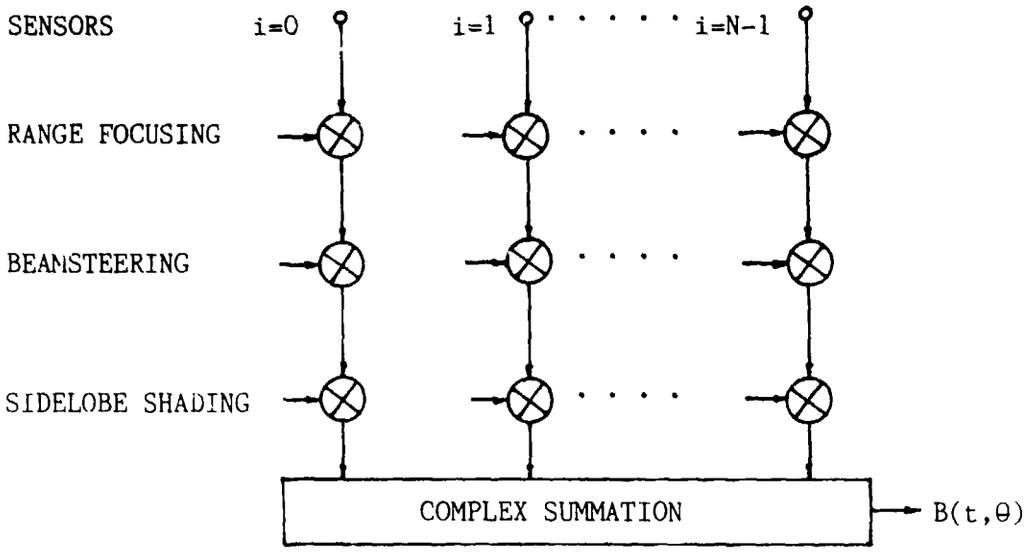

Figure 2-4. Single frequency beamformer output (steered, focused, and shaped).
(Adapted from reference 16, page 9)

input signals to k sets of weights, where k equals the number of beams desired, and then summing the results in k summers to produce k beams at the output.

For orthogonal multiple beamforming, the following development applies.

If the phase delay of the input signal is represented relative to sensor 0 rather than sensor n-1, then the input signal at any element sensor is

$$S_i = e^{j(\omega t + i\phi)} \quad . \qquad 2\text{-}16$$

Thus, the beamsteering coefficient is now in the form

$$C_i = e^{-ji\phi} \quad . \qquad 2\text{-}17$$

The phase delay ϕ can be represented by a time delay τ by the following transformation:

$$\phi = \frac{2\pi d}{\lambda} \sin\phi \quad , \text{ where } \lambda = c/f \quad , \text{ so that}$$

$$\phi = \frac{2\pi f d}{c} \sin\phi = \omega\left(\frac{d}{c} \sin\phi\right) \quad . \qquad 2\text{-}18$$

Letting $\tau = \frac{d}{c} \sin\phi$, where $c = 3 \times 10^8$ m/s, then

$$C_i = e^{-} = e^{-ji\omega\tau} \quad . \qquad 2\text{-}19$$

The beamformer output from Figure 2-4 was

$$B(t,\phi) \sum_{i=0}^{n-1} W_i S_i e^{jkx_i^2/2R(t)} e^{-j(i-n+1)\phi} \quad .$$

If the input signal, sidelobe shading, and range focusing are combined to form A_i, and the new beamsteering coefficient (2-19) is used, then

$$B(t,\phi) = \sum_{i=0}^{n-1} A_i e^{-ji\omega\tau} \quad . \qquad 2\text{-}20$$

This complex summed signal has the same form as the discrete inverse Fourier Transform

$$F(k) = \sum_{n=0}^{n-1} f(n) e^{-j(2\pi/n)nk} \quad , \qquad 2\text{-}21$$

where $F(k)$ is analogous to $B(t,\phi)$, $f(n)$ is analogous to A_i, and $(2\pi/n)nk$ is analogous to $i\omega\tau$. This has importance because aperture space can be transformed to beam space using a Fourier transformation. Therefore, an array with N aperture elements can produce N beams. To produce N beams from N sensor elements, the following scheme can be employed:

The γth beam is represented as

$$B(t,\phi^{\gamma}) = \sum_{i=0}^{N-1} A_i(t) e^{-j(i\omega\tau^{\gamma})} = \sum_{i=0}^{N-1} A_i(t) e^{-j(2\pi\gamma i/N)}, \qquad 2\text{-}22$$

$$\gamma = 0,1,2,\ldots,N-1.$$

$$B(t,\theta^0) = A_0 + A_1 + A_2 + \ldots + A_{N-1}$$

$$B(t,\theta^1) = A_0 + A_1 e^{-j(2\pi/N)} + A_2 e^{-j(4\pi/N)} + \ldots + A_{N-1} e^{-j(\frac{2\pi(N-1)}{N})}$$

$$B(t,\theta^{N-1}) = A_0 + A_1 e^{-j(\frac{2\pi(N-1)}{N})} + \ldots + A_{N-1} e^{-j(\frac{2\pi(N-1)^2}{N})} \quad . \quad 2\text{-}23$$

Each beam is centered on θ^γ, where

$$\theta^\gamma = \sin^{-1}[\frac{\lambda\gamma}{Nd}] \quad , \lambda = 0, 1, \ldots, N-1.$$

The beams formed further away from the boresight axis tend to have broader beamwidth. This effect is approximated by the relationship:

$$BW_{3dB} = .886(\frac{\lambda}{Nd}) \sec\theta \qquad \text{near broadside.} \qquad 2\text{-}24$$

The endfire beamwidth is larger than the broadside beamwidth by a factor of

$$\frac{BW_{3dB(Endfire)}}{BW_{3dB(Broadside)}} \sim 2[.885(\lambda/Nd)]^{1/2} \quad . \qquad 2\text{-}25$$

Beam broadening away from the boresight axis increases sidelobes and limits the total angle of space that can be covered (i.e., the summed beamwidth) to approximately $\pm 60°$. Within this beamwidth, it may be desired to have as many beams as feasible since as the number of beams increases, the individual beamwidth decreases. Thus, angular

resolution decreases, allowing better separation of targets in close proximity.

An economical application of the Discrete Fourier Transform (DFT) is the Fast Fourier Transform (FFT). This is an algorithm which takes the set of N equations (2-23) given above, and produces N beams, requiring only $2N[(LOG_2N)-3]+8$ real multiplications (for the Cooley-Tukey Radix-2 FFT). A straight forward DFT, in comparison, would require approximately N^2 multiplications.

It must be stressed that all beamforming discussed thus far for linear arrays is frequency sensitive. The lowest sidelobes occur when the inter-element spacing is set at $\lambda/2$, in reference to the operating frequency. If a different frequency is used, the spacing is no longer $\lambda/2$, and sidelobes increase in size and number. The main lobe beamwidth is also changed. This in turn changes the angular resolution (for the worse). Therefore, the phased-array, as described above, is a single frequency system.

2.5 OVERALL SIGNAL FLOW

Having looked at basic beamforming for an equally spaced linear array for both single-beam and multiple-beam, the signal flow for digital beamforming, complete with errors, will now be examined.

The input signal from a single element is

$$V_n(t) = A_n\cos(\omega t+\tau_n) + \eta(t)\cos\omega t, \qquad 2\text{-}26$$

where η is the Gaussian noise with variance σ^2. After conversion to baseband and separation into in-phase and quadrature components, the signal is

$$V_n(t) = I_n(t) + Q_n(t) = A_n\cos\tau_n + \eta_{i_n}(t) + A_n\sin\tau_n + \eta_{Q_n}(t). \quad 2\text{-}27$$

Including mismatches in the in-phase and quadrature mixers, which produce phase error S_n and gain error K_n, results in

$$I_n(t) = A_n(\cos\tau_n - 1/2\ S_n\sin\tau_n + 1/2\ K_n\cos\tau_n) + \eta_{I_n}(t) \quad 2\text{-}28$$

$$Q_n(t) = A_n(\sin\tau_n - 1/2\ S_n\cos\tau_n - 1/2\ K_n\sin\tau_n) + \eta_{Q_n}(t). \quad 2\text{-}29$$

Let these mismatches be defined as

$$\frac{\xi_{I_n}}{A_n} = -1/2\ S_n\sin\tau_n + 1/2\ K_n\cos\tau_n, \text{ and} \quad 2\text{-}30$$

$$\frac{\xi_{Q_n}}{A_n} = -1/2\ S_n\cos\tau_n - 1/2\ K_n\sin\tau_n. \quad 2\text{-}31$$

Then

$$I_n(t) = A_n\cos\tau_n + \xi_{I_n} + \eta_{I_n}(t) \quad , \text{ and} \quad 2\text{-}32$$

$$Q_n(t) = A_n\sin\tau_n + \xi_{Q_n} + N_{Q_n}(t) \quad . \quad 2\text{-}33$$

At this point, the signals are sampled at a maximum rate of 1.4B, where B is the bandwidth or spectral width of the radar pulse, and digitized.

2.6 DEVELOPMENT OF WEIGHTING COEFFICIENTS

Let the complex weighting term be defined as

$$W = I_w + jQ_w = C\cos\theta + jC\sin\theta, \qquad 2\text{-}34$$

and the received signal be

$$x_n = I_n + jQ_n = S_n - \Delta S_n + \eta_n, \qquad 2\text{-}35$$

where

$$S_n = A_n \exp(j\tau_n), \quad \Delta S_n = \xi_{I_n} + j\xi_{Q_n}, \quad \text{and} \quad \eta_n = \eta_{I_n} + j\eta_{Q_n}.$$

Then

$$x'_n = WX_n = (I_n I_w - Q_n Q_w) + j(I_n Q_w + I_w Q_n) \quad . \qquad 2\text{-}36$$

Note that four real multiplications and two additions are required for one complex multiplication. Due to quantization errors in forming weights, we define

$$W'_n X_n = (W_n - \Delta W_n)(S_n - \Delta S_n + N_n)$$

$$= W_n S_n - W_n \Delta S_n + W_n \eta_n - S_n \Delta W_n + \Delta W_n \Delta S_n - \Delta W_n \eta_n$$

$$\simeq W_n S_n - W_n \Delta S_n + W_n \eta_n - S_n \Delta W_n, \qquad 2\text{-}37$$

where

$$\langle |\Delta W_n|^2 \rangle = (1/6)\, 2^{2(1-b_w)} \text{ (weighting quantization error)}, \qquad 2\text{-}38$$

$$\langle |\eta_n|^2 \rangle = 2[\sigma^2 + (1/12)q^2] \text{ (signal noise and quantization error)}, \qquad 2\text{-}39$$

and

$$\langle |\Delta S_n|^2 \rangle = (1/4)\, A^2{}_n (S^2{}_n + K^2{}_n) \text{ (signal mismatch error)}. \qquad 2\text{-}40$$

In the above equations, b_w is the number of bits in the weighting word, and q is a single step of quantized voltage.

The signals and weights for the whole linear array can be expressed as the vectors

$$S^T = [S_1, S_2, \ldots, S_n] \quad ,$$

$$W^T = [W_1, W_2, \ldots, W_n] \quad ,$$

$$\Delta S^T = [\Delta S_1, \Delta S_2, \ldots, \Delta S_n] \quad ;$$

$$\Delta W^T = [\Delta W_1, \Delta W_2, \ldots, \Delta W_n] \quad ,$$

$$H^T = [\eta_1, \eta_2, \ldots, \eta_n] \quad \text{and}$$

$$X^T = [X_1, X_2, \ldots, X_n] \quad .$$

In vector form, the beamformer output is

$$\Omega = W^{1T}X(1+\rho) = (W+\Delta W)^T(S+\Delta S+H)(1+\rho),$$

$$\simeq W^TS + W^T\Delta S + W^TH + \Delta W^TS + \rho W^TS, \qquad 2\text{-}41$$

where ρ is word length truncation error. The first term, W^TS, represents the desired beamformer output. The next four terms represent first order errors.

Different weighting distributions, such as Dolph-Chebyshev coefficients or Hamming coefficients, may be used to control, in general, the sidelobe response. Adaptive weighting, as well, can steer beams and nulls, or reduce sidelobes as a result of self calibration, or modify the beam shape. Figure 2-5 shows the effects of various errors in a digital beamformer for a Hamming weighting distribution for N channels.

2.7 SOURCES OF ERROR

Thermal noise is generated by receiver components. It is Gaussian in nature and has power equal to its variance σ^2.

Coding or quantization error tends to vary in a sawtooth manner in the absence of thermal noise. As the level of thermal noise increases,

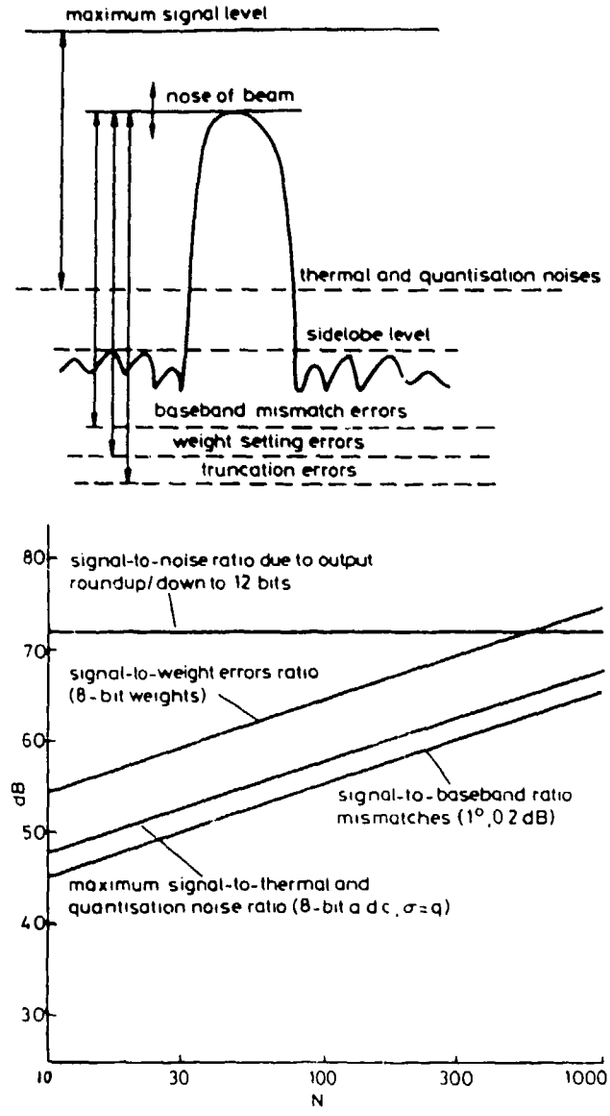

Figure 2-5. Effects of various errors in a digital beamformer for hamming weighting against N channels. (Taken from reference 2, page 272)

the quantization error is reduced. For $\sigma \geq .5q$, the error is negligible and can be combined linearly with the thermal noise. The quantization error range is assumed to be between -1/2q and 1/2q, so that the mean square error is

$$\int_{-.5q}^{.5q} [X^2/q]\, dx = (1/12)q^2 \ . \qquad 2\text{-}42$$

Therefore, the net average noise power (thermal and quantization) is

$$\langle |\eta_n|^2 \rangle = 2[\sigma^2 + (1/12)q^2] \qquad 2\text{-}39$$

in each channel.

I and Q mixer mismatches were defined in Equations 2-30 and 2-31, which lead to the combined signal mismatch error power of Equation 2-40, $(1/4)A^2_n(S^2_n + K^2_n)$.

There are phase and amplitude errors between elements, as well as coupling errors (discussed in Chapter One). These are not to be confused with the mismatches between I and Q channels of a single element. Errors may result if individual elements malfunction or quit. It was described earlier how a digital self-calibration can compensate for these errors. With adaptive beamforming, the null depths are not affected by these errors.

If a radar system is airborne, and thus on a moving platform, linearity errors can result. Harmonic inter-modulation due to doppler effect on clutter creates non-linear distortion at the harmonics of the frequency offset error, which can be a serious problem for analog

systems. Mathews points out that digital beamformers are much more tolerant and that design criteria may be relaxed [17].

CHAPTER 3

CURRENT TECHNOLOGY

3.0 INTRODUCTION

Systems currently being developed using digital techniques are experimental in nature and are assessing the directions in which to proceed in order to reap the most benefits at an ''affordable'' price. A comparison of the five systems discussed is found in Table 3-1.

3.1 STANDARD TELECOMMUNICATIONS LABORATORIES

Standard Telecommunications Laboratories, Limited (situated in Harlow, Essex, England) jointly with ITT Gilfillan (in USA) have an experimental system for adaptive digital beamforming [2]. Their system is designed to reject jamming on a vertical pattern. A null is directed toward the jammer while maintaining coverage above and below this angle. A vertical, receive-only, linear array of eight horns covers a 20° azimuthal sector and operates in the L-band (1-2 GHZ). The rotating test radar operates normally until the designated 20° sector is reached. At this point, the normal receive circuits are switched to the eight-horn digital receivers. The eight inputs are digitized, adaptively weighted, and summed in 2 μs. The system sampling time is 6 μs, providing a more than ample margin.

TABLE 3-1

COMPARISON OF EXPERIMENTAL SYSTEMS' CHARACTERISTICS

SYSTEM	ADAPTIVE NULLING	SELF CALIBRATION	MULTIPLE BEAMS	SUBARRAYS USED	BITS IN ADC	RECEIVE ELEMENTS	BANDWIDTH (APPROXIMATE)	DYNAMIC RANGE (MAX)
STL/ITT	YES	NO	NO	NO	8	8	120 KHZ	51 dB
ELRA	YES	YES	YES (6)	YES (48)	10	768	100 KHZ	70 dB
GASP	YES	YES	NO	NO	12	32	240 KHZ	81 dB
CONUS B-OTH	YES	NO	YES (4)	?	?	82	100 KHZ	?
RADC	NO	YES	NO	?	?	32	500 KHZ	?

3.2 ELRA

The ELRA experimental phased array radar is located at FFM (Forschungsinstitut Fur Funk und Mathematik) in the Federal Republic of Germany [18,1]. There are separate arrays for transmitting and receiving. The antennas are S-band circular thinned phased arrays. There are 300 transmit elements with a 1:8.2 fill factor and 768 receive elements with a 1:6.25 fill factor. The system uses analog phase shifters at each receive element, which output in-phase and quadrature components. Element signals are then summed into 48 sub-arrays of 16 channels each, and at this point digitized. The A.D.C. operates at a 2MHZ rate. Three fixed beams (one sum beam and two difference beams) are obtained. Adaptive weighting and beamforming is not done at present, but system expansion to allow for it is planned.

The transmitter provides a 2-μs tracking pulse and a 10-μs search pulse. Since the sampling time is .5 μs, enough time is available to generate six independent beams by a time-multiplex method. This rapid steering to six different directions gives the appearance of having six simultaneous beams.

Self-calibration is accomplished by an auxiliary antenna probe in the near-field. The phase and gain of each element is evaluated and the phase information used in the control of the phase shifters. Faulty elements with insufficient gain or excessive phase error are identified for future repair. A complete check of all transmit and receive elements takes approximately 10 seconds.

3.3 GASP

The GEC array-signal-processing (GASP) test bed is an experimental linear phased array receiving system at the Marconi Research Centre in Chelmsford, Essex, U.K. [19]. This system will have 32 elements when completed. As of 1985, 25 elements have been interfaced, and the results presented by Old (et.al) are based on 16 elements operating at S-band (3 GHZ). GASP uses a fully digital implementation. The received signal is down-converted to in-phase and quadrature baseband signals, digitized in 12-bit ADC's at a 3-μs sampling rate. The digital signals are now available to a control computer, a sample store (2048 word memory for off-line processing), and the real-time beamformer. The beamformer produces an output expressed by

$$\text{Array Output} = \sum_{n=0}^{n-1} D_n \cdot W_n \cdot S_n \cdot C_n \quad , \qquad 3\text{-}1$$

where

D_n = Incoming signal from nth element,

W_n = The weighting coefficient,

S_n = The beamsteering coefficient, and

C_n = The correction coefficient.

This flexible system can accept fixed weighting coefficients (such as Hanning and Hamming), or calculate them based on user-supplied parameters (such as Taylor or Dolph-Chebychev).

GASP also incorporates self-calibration using a far-field probe or couplers placed between the elements and receivers. Phase and gain errors are calculated using 512 time samples input to an FFT. The results are used to form and store the correction coefficients, C_n's.

This highly flexible system will enable a wide range of experiments in digital signal processing and calibration techniques.

3.4 CONUS B-OTH

This continental United States bistatic backscatter over-the-horizon radar is built by the General Electric Company [1]. Bistatic radar has its transmitter and receiver located in different geographical locations. It is a low-frequency radar (between 6-20 MHZ) with a bandwidth of about 100 KHZ. 82 receive elements are used to form four simultaneous beams covering the transmitted beamwidth. Adaptive nulling and on-line receiver error correction are performed.

3.5 RADC

The Rome Air Development Center in Bedford, Massachusetts, is testing a 32-element array at C-band (4-6 GHZ) [1]. This system has a 500 KHZ bandwidth. Self-calibration through feedback to the element front-ends should provide very low sidelobe patterns.

3.6 GENERAL HARDWARE REQUIREMENTS FOR FULL DIGITAL IMPLEMENTATION

The main limitations to digital beamforming are speed, complexity and cost. Even analog phased array systems have, for the most part, been restricted to military use where mission requirements were more important than complexity and cost. Much work is being done (such as monolithic microwave integrated circuits - MMIC's) to reduce the size and cost of these systems, while increasing component and processing speed. As the overall cost of phased array systems is reduced, digital beamforming will also become more attractive.

In the receiving channels of a digital beamformer, the phase shifters are replaced by digital weighting coefficients which combine with the element input signal after analog-to-digital conversion. The ADC and the number of elements set the limits on dynamic range, $[6(B-1)+10 \log_{10}N]$, and the bandwidth, $(f_{sampling}/1.4)$. Presently available ADC's are:

12-bit, 5-MHZ ADC from Analog Devices on 5'' x 7'' board [21],

12-bit, 2-MHZ ADC from ILC Data Device on 40-PIN DIP [22],

8-bit, 50-MHZ ADC [1].

These would limit bandwidths to 3.5 MHZ for 12-bit and 35 MHZ for 8-bit ADC's.

The beam pattern controller determines the adaptive and corrective weights to apply to the input signals. The processing speed is determined by the algorithms used and the number of signal elements in the array. An important consideration here is how often the weights need updated, which for adaptive nulling depends on the rate of change in position of airborne jammers. Early digital beamformers will work

with ''acceptable'', not ''optimal'', update rates. The choice of Hung's and Turner's algorithm would appear to give the fastest throughput. For nulling 10 jammers with a 100-element array, the SMI method requires a million multiplications. The Hung and Turner algorithm requires less than 50,000 multiplications. If updates were needed 10 times a second, then total multiples are less than 500,000/sec, which is easily handled by a fast dedicated processor. Even 2,000 elements would need only 10 million operations per second, which is still realizable on a central processor [1]. Larger arrays may also be handled by sub-arraying techniques to reduce the computational load.

The beamformer must multiply the individual signals by the most recent weights, steering coefficients, and corrective coefficients, and then sum them into the final beam output. This requires ($4Nkf_r$) real multiplications, where N is the number of elements, k is the number of simultaneous beams, and f_r is the sampling frequency. One beam formed with 64 elements at a 1-MHZ sampling rate requires $4 \times 64 \times 1 \times 10^6 = 256 \times 10^6$ operations per second. Present processors can handle this, but not if thousands of elements form the array. Several alternatives are possible. The first is placing a digital signal processor in each input channel to do all or most of the multiplication. Texas Instruments has for sale a 16-bit x 16-bit parallel multiplier/accumulator, the Tact 1010-65, which multiplies and adds in 65 ns [23]. This allows for a 3.8 MHZ sampling rate if four multiplies are performed at each channel.

Another alternative is using a Fast Fourier Transform (FFT) processor, which simultaneously forms a set of N beams from N signal

inputs, requiring $\{2N[(LOG_2N)-3]+8\}$ multiplications per sample. As long as $N \leq 2000$, the FFT takes fewer operations than forming four beams using arbitrary weights. For the case of 64 elements, forming 64 beams requires 392×10^6 operations per second for a 1-MHZ sampling rate.

As seen in Table 3-1, limits in processing speeds have kept the number of array elements low (below 100 after sub-arraying) and the bandwidth small (less than 0.5 MHZ) on the current experimental systems.

CHAPTER 4

FUTURE TRENDS

4.0 POSSIBLE SYSTEMS

The systolic array discussed in Chapter 1 may soon find application where the bandwidth is small (as in sonar), due to processing node speeds, and where the number of elements is limited. For example, a 10-element array would need 55 signal processors, while a 50-element array would need 1,465 processors. As progress continues in making smaller, faster, and less expensive signal processors, systolic arrays may find their way into a number of least mean square error applications. Some experimental work is being done for adaptive beamforming in the U.K. [24] and by RCA in the U.S. [25].

4.1 INTEGRATED CIRCUIT TECHNOLOGY

The push for single chip circuits that are smaller, faster, and of lower cost continues in both silicon and Gallium Arsenide (GaAs) [26]. GaAs logic is now available at speeds up to 3 GHZ, and this is expected to increase rapidly. HP's C. House predicts that todays high-price 6-bit 1-GEZ ADC will be a low-cost 10-GHZ ADC by 1994. NEC will soon be offering a digital signal processor (DSP) chip with 32-bit

floating point operations and a 150 ns cycle time. Even faster cycle times and inexpensive parallel processing will be needed.

A marriage of monolithic analog circuits with high speed digital circuits may be able to draw from the best of both domains.

CHAPTER 5

CONCLUSION

Tremendous steps have been taken in making digital beamforming a realizable method of achieving a highly flexible and responsive system in the presence of rapidly changing noise and jamming conditions. Although it may be the year 2000 before full digital implementation is feasible and cost effective, sub-arraying techniques will allow some of the benefits to be employed before then. Self-calibration may be used sooner to achieve lower sidelobes since it is not as restricted by processing times. For now, digital beamforming will be restricted to systems of few elements (probably less than 100) and small bandwidth (of about 100 KHZ).

Three areas of research and advancement will hasten the advent of widespread digital beamforming: work on the speed, size, and cost of ICs, the development of creative architectures to maximize data throughput, and the development of refined and new algorithms to reduce processing times.

BIBLIOGRAPHY

1. H. Steyskal, ''Digital Beamforming Antennas, An Introduction,'' Microwave Journal, pp 107-124, Jan., (1987)

2. P. Barton, ''Digital Beamforming for Radar,'' IEE Proc., Vol. 127, Pt. F, No. 4, pp 266-277, (1980)

3. S. P. Applebaum, ''Adaptive Arrays,'' IEEE Trans. on Antennas and Propagation, Vol. AP-24, No. 5, pp 585-598, (1976)

4. E. C. Jordan, ed., Reference Data for Engineers: Radio, Electronics, Computer, and Communications, 7th Ed., Howard W. Sams Co., Inc., New York, pp 32.42-32.43, (1985)

5. B. Widrow, P. E. Mantley, L. J. Griffiths, and B. B. Goode, ''Adaptive Antenna Systems,'' Proceedings of the IEEE, Vol. 55, No. 12, pp 2143-2159, (1967)

6. I. S. Reed, J. D. Mallett, and L. E. Brennan, ''Rapid Convergence Rate in Adaptive Arrays,'' IEEE Trans. on Aerospace and Electronic Syst , Vol. AES-10, No. 6, pp 853-863, (1974)

7. E. K. L. Hung and R. M. Turner, ''A Fast Beamforming Algorithm for Large Arrays,'' IEEE Trans. on Aerospace and Electronic Systems, Vol. AES-19, No. 4, pp 598-607, (1983)

8. P. J. Hargrave and C. R. Ward, ''New Approach to Adaptive Beamforming,'' Electrical Communication, Vol. 59, No. 3, pp 300-305, (1985)

9. C. R. Ward, P. J. Hargrave, and J. G. McWhirter, ''A Novel Algorithm and Architecture for Adaptive Digital Beamforming,'' IEEE Trans. on Antennas and Propagation, Vol. AP-34, No. 3, pp 338-346, (1986)

10. M. I. Skolnik, Introduction to Radar Systems, McGraw-Hill Book Co., New York, pp 310-337, (1980)

11. L. Sheats, ''Fast Fourier Transform,'' Radar Technology, E. Brookner, ed., Artech House, Inc., Massachusetts, pp 149-154, (1985)

12. J. S. Ward, P. Barton, J. B. G. Roberts, and B. J. Stanier, ''Figures of Merit for VSLI Implementations of Digital Signal Processing Algorithms,'' IEE Proc., Vol. 131, Pt. F, No. 1, pp 64-70, (1984)

13. E. Brookner, ed., Radar Technology, Artech House, Inc., Massachusetts, pp 181, (1985)

BIBLIOGRAPHY (Continued)

14. J. A. Johnston, ''Parallel Pipeline Fast Fourier Transformer,'' IEE Proc., Vol. 130, Pt. F, No. 6, pp 564-572, (1983)

15. V. Nickel, ''Angular Superresolution with Phased Array Radar: A Review of Algorithms and Operational Constraints,'' IEE Proc., Vol. 134, Pt. F, No. 1, pp 53-59, (1987)

16. F. Ingels, ''Array Fundamentals, A Tutorial,'' Unpublished, (1987)

17. B. D. Mathews, ''Nonlinearities in Digital Manifold Phased Arrays,'' IEEE Trans. on Antennas and Propagation, Vol. AP-34, No. 11, pp 1346-1355, (1986)

18. W. Sander, ''Experimental Phased-Array Radar ELRA: Antenna System,'' IEE Proc., Vol. 127, Pt. F, No. 4, pp 285-289, (1980)

19. J. C. Old, D. J. Day, and G. N. Harvey, ''GASP - The GEC Array-Signal-Processing Test Bed,'' IEEE 1985 International Radar Conference, New York, pp 220-225, (1985)

20. W. Sander, ''Monitoring and Calibration of Active Phased Arrays,'' IEEE 1985 International Radar Conference, New York, pp 45-51, (1985)

21. C. Pell, A. C. Fairhead, and M. B. Thomas, ''VHPIC for Radar,'' Advanced Signal Processing, D. J. Creasey, ed., Peregrinus, Ltd., (IEE), pp 221-231, (1985)

22. F. Goodenough, ''Focus on Hybrid A-D Converters,'' Electronic Design, pp 191-196, Oct. 17, (1985)

23. Texas Instrument Product News Sheet on TI-TACT1010-65 parallel multiplier/accumulator, (1987)

24. J. V. McCanny and J. G. McWhirter, ''Some Systolic Array Developments in the United Kingdom,'' Computer, (IEEE), Vol. 20, No. 7, pp 51-63, (1987)

25. C. E. Hein, R. M. Zieger, and J. A. Urband, ''The Design of a GaAs Systolic Array for an Adaptive Null Steering Beamforming Controller,'' Computer, (IEEE), Vol. 20, No. 7, pp 92-93, (1987)

26. E. Brookner, ''Array Radars: An Update, Part II,'' Microwave Journal, pp 167-174, Mar., (1987)